Electronic Supplementary Material (ESI) for Nanoscale.

Supporting Information

for

Effects of dielectric screening on the excitonic and critical points properties of WS_2/MoS_2 heterostructures

Xudan Zhu,[a] Junbo He,[a] Rongjun Zhang,*[a] Chunxiao Cong,*[b] Yuxiang Zheng,[a] Hao Zhang,[a] Shanwen Zhang,*[c] and Liangyao Chen[a]

[a]*Key Laboratory of Micro and Nano Photonic Structures, Ministry of Education, Shanghai Engineering Research Center of Ultra-Precision Optical Manufacturing, School of Information Science and Engineering, Fudan University, Shanghai 200433, China. Email: rjzhang@fudan.edu.cn.*

[b]*State Key Laboratory of ASIC and System, School of Information Science and Engineering, Fudan University, Shanghai 200433, China. Email: cxcong@fudan.edu.cn.*

[c]*Grating Technology Laboratory, Changchun Institute of Optics and Fine Mechanics and Physics, Chinese Academy of Sciences, Changchun, Jilin 130033, China. Email: zhshwen007@163.com.*

1. Atomic Force Microscope (AFM) Results

The AFM images are shown in Fig. S1a-c, demonstrating that there is no discernible contaminations on the surface of the transferred 1L-WS_2, 1L-MoS_2, and WS_2/MoS_2 heterostructure.

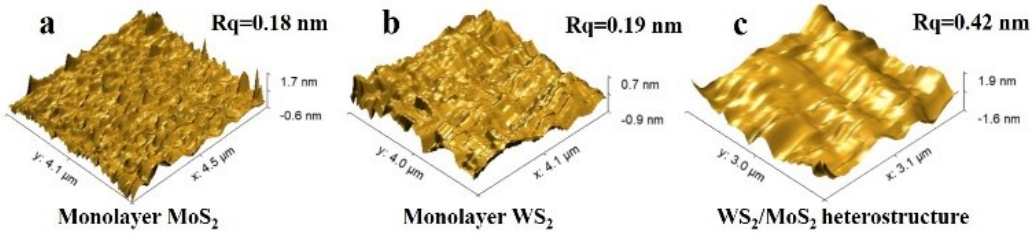

Fig. S1 AFM images and surface roughness R_q of the (a) 1L-MoS_2 (b) 1L-WS_2 and (c) WS_2/MoS_2 heterostructure.

2. Photoluminescence (PL) Spectra Analysis

2.1 PL Spectra of Sapphire Substrate

Fig. S2 shows the PL spectra of the sapphire substrate. Specifically, a spiculate peak at 1.79 eV is observed.

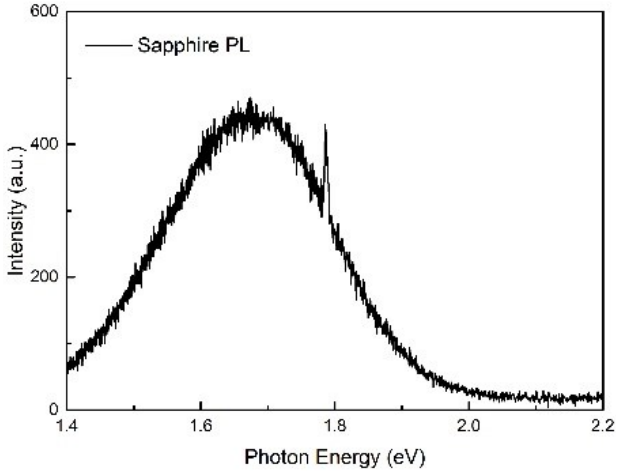

Fig. S2 Photoluminescence Spectra of Sapphire Substrate.

2.2 PL Spectra of 1L-MoS_2, 1L-WS_2, and WS_2/MoS_2 heterostructure

Specially, in 2D materials the energies of PL peaks are corresponding to the transition energies of excitonic ground state (n=1, i.e., optical bandgap).[1, 2] Note that, n is the principal quantum number of the bound states of the excitons. This is the Wannier-Mott excitons model, which analogous to hydrogen atom model.[3-5]

Fig. S3 shows the PL Spectra of 1L-MoS_2, 1L-WS_2, and the WS_2/MoS_2 heterostructure. The energies of neutral A excitons (X_A) of 1L-MoS_2 and 1L-WS_2 is 1.85 eV and 2.00 eV, respectively. These two direct transitions in 1L-TMDs occur between the VBM and CBM, locating at K point (high-symmetry points along the six equivalent [111] directions of the Brillouin zone (BZ)[3]) according to the previous theoretical studies.[6-8] Additionally, the charged excitons (trions) of 1L-WS_2 and 1L-MoS_2 are found (labelled as X_A^-), whose binding energy can be experimentally extracted from the separation of neutral exciton energy from trion energy in PL.[9] Thus, the trion binding energies of 1L-MoS_2 and 1L-WS_2 are 35.8 and 49.6 meV, respectively, which is in agreement with recent literature.[10] While, in the case of WS_2/MoS_2 heterostructure, the trion PL peak of 1L-WS_2 overlaps with neutral A exciton PL peak of MoS_2. Thus, only four typical peaks have been obtained by Gaussian fitting, with increasing energy, the peaks are assigned to interlayer exciton (1.60 eV), 1L-MoS_2 trion (1.79 eV), 1L-MoS_2 A exciton (1.87 eV), and 1L-

WS_2 A exciton (2.00 eV). The photoexcitation carriers transferring across layers will consume the neutral excitons in either layer,[11] which results in the PL quenching in heterostructure film, as seen in Fig. S3.[12, 13]

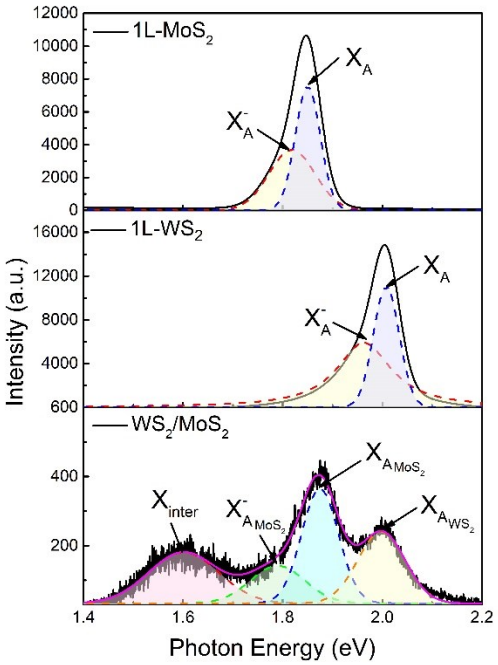

Fig. S3 PL spectra of 1L-WS_2, 1L-MoS_2, and WS_2/MoS_2 heterostructure excited by a 532 nm laser under room temperature, where the detailed mutiple peaks were obtained by Gaussian fitting. And, before plotting the PL spectra of 1L-WS_2, 1L-MoS_2, and WS_2/MoS_2 heterostructure, sapphire substrate PL spectra (shown as Fig. S2) has been subtracted.

3. Point-by-point Method Fitting Ellipsometric Parameters

3.1 Optical model

The original ellipsometric parameters were fitted using point-by-point method with a vertical stacked optical model consisting of sapphire substrate/thin film samples/air ambient. And the thickness of substrate, 1L- transition metal dichalcogenides (TMDs), WS_2/MoS_2 heterostructure films were set as 1 mm, 0.65 nm, and 1.3 nm, respectively. These are the typical theorical thickness of 1L-TMDs films. In addition, the surface roughness and possible interlayer air gap was neglected while fitting procedure. As shown in Fig. S4a-c, in order to guarantee the accuracy of the fitting results, we used different thickness around the classic value to fit the dielectric spectra of the films. While different thickness only results in the fluctuation of the dielectric constant values, which is not focused here. And the peak positions are fixed. Thus, the choice that using typical thickness values can be implemented.

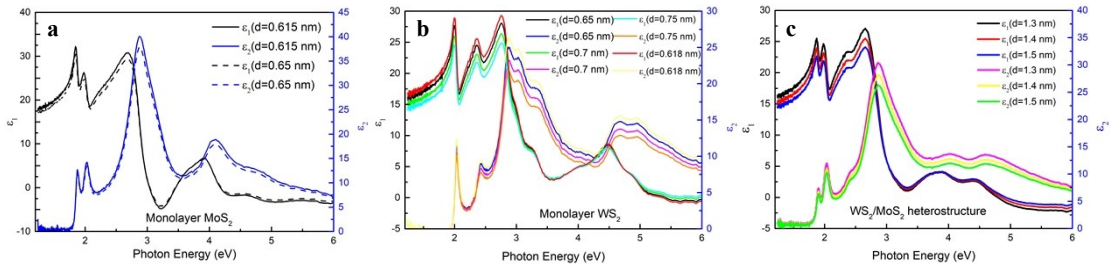

Fig. S4 The complex dielectric function spectra of (a) monolayer MoS_2; (b) monolayer WS_2; (c) WS_2/MoS_2 heterostructure films fitted by point by point method using different film thickness.

3.2 Self-Check Procedure

What we must expressed is that the point-by-point method is mathematical inversion at each measured point of the SE data, lacking of physical constraints.[14] Hence, a self-check procedure is necessary. There are three powerful evidence to verify the accuracy of the fitting results:

First, as shown in Fig. S5, the measured experimental data (unfilled symbols) and calculated data (solid lines) perfectly match in the samples.

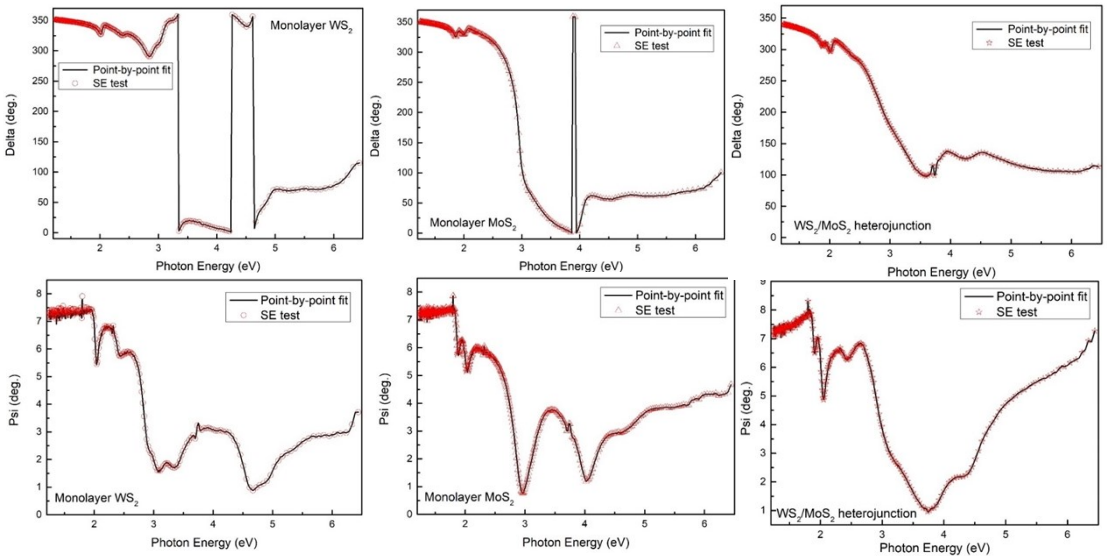

Fig. S5 The experimental (unfilled symbols) and calculated data (solid lines) of the ellipsometric parameters (ψ and Δ) for monolayer TMDs and the heterostructure thin film.

Second, the agreement of our 1L-TMDs optical conductivity results and those of previous study[15] revealing the reliability of our fitting results. Fig. S6a shows the calculated real part of the complex film conductivity profile of the 1L-TMDs and WS_2/MoS_2 heterostructure. And the complex film conductivity was calculated from complex dielectric functions using equation (1) and (2):[15]

$$\sigma(E)=\sigma_1(E)+\mathrm{j}\sigma_2(E)=-\mathrm{j}\frac{\varepsilon_0 E}{\mathrm{h}}\left[\varepsilon(E)-1\right] \tag{1}$$

$$\sigma^{\mathrm{F}}(E)=\sigma_1^{\mathrm{F}}(E)+\mathrm{j}\sigma_2^{\mathrm{F}}(E)\equiv\sigma(E)d \tag{2}$$

where σ, E, ε, σ^{F}, and d denote the complex optical conductivity, photon energy, complex dielectric function (shown as Fig. 2a in the paper), the real part of complex film conductivity (shown as Fig. 2b in the paper), and film thickness (use the same values as ellipsometric data fitting), respectively. The real part of the complex film conductivity (in units of $G_0 = 2e^2/h$) of all sampes were plotted in Fig. S6a, where the data of 1L-TMDs from previous studies[15] were extracted for comparing. As expected, the peaks of our data agrees well with the previous results. While, the amplitude of our results are slightly different from that of the prevous study[15], which can be attibuted to different sythesis methods of the samples. Meanwhile, the optical conductivity curves of our monolayer samples present better *Step funtion* feature compared with the previous results, revealing the higher quality of our samples. Addionally, the discussion of optical conductivity of the samples is implemented in the paper.

Third, the consistency of peaks in the absorbance ($A(E)$) and absorption coefficient spectra ($\alpha(E)$) of the 1L-TMDs and WS_2/MoS_2 heterostructure films, calculated repectively using equation (3)[16] and (4)[14], can guarantee the accuracy of the fitting results. And the $A(E)$ and $\alpha(E)$ of the three samples are compared in Fig. S6b. Notably, the absorbance ($A(E)$) in transmission spectroscopy is defined as the logarithm of the ratio of the intensity of radiation prior to the sample (I_0) and the radiation intensity after the sample (I). And the T represents the transmission spectra, which was measured by spectrophotometer with the wavelength range from 360 to 1100 nm under room temperature.

$$A=\log(\mathrm{I}_0/\mathrm{I})=-\log(\mathrm{T}) \tag{3}$$

Moreover, the absorption coefficient spectra ($\alpha(E)$) of the samples are derived from the complex dielectric functions, shown as Fig. 2a in the paper, using equation (4):[14]

$$\alpha=\frac{4\pi k}{\lambda}=\frac{4\pi}{\lambda}\left[\frac{-\varepsilon_1+\left(\varepsilon_1^{\,2}+\varepsilon_2^{\,2}\right)^{1/2}}{2}\right]^{1/2} \tag{4}$$

Meanwhile, $A(E)$ is in proportion to $\alpha(E)$, which can explain that the peaks of two spectra are located in the same energies but with different amplitude, as revealed in Fig. S6b. And the absorption edges of the fitted curves in Fig.

S6b are reasonable.

Fourth, the spectral features of ε_1 can correspond to those of ε_2, shown as Fig. 2a in the paper, indicating that the fitting data satisfy the Kramers-Kronig constrained relationship. In addition, there are no abrupt peaks superimposing on the smooth dielectric function background.

In conclusion, our fitting results are reliable.

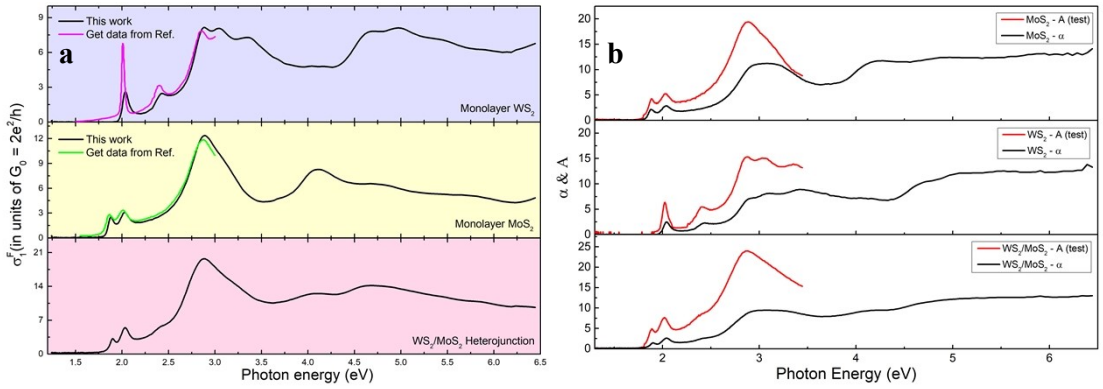

Fig. S6 Plots of (a) the real part of the complex film conductivity (in units of $G_0 = 2e^2/h$) and (b) the absorbance ($A(E)$, red lines) and absorption coefficient spectra ($\alpha(E)$, black lines) of the 1L-TMDs and WS_2/MoS_2 heterostructure films. And the color lines (puple and green lines) in top two panels of (a) were obtained from previous study[15] using GetData Graph Digitizer sorftware.

4. Critical Points Fitting

The CPs properties were obtained by fitting the second derivative of the complex dielectric functions (real and imaginary parts simultaneously) with respect to photon energy ($d^2\varepsilon/dE^2$), wherein n took -1. Fig. S7b depicts the experimental (solid lines; obtained by numerical differentiation of the data provided in Fig. 2a in paper) and best-match curves (unfilled symbols; calculated using equation (5) in paper) for $d^2\varepsilon/dE^2$. As showed in Fig. S7b, they are in excellent agreement, indicating the accuracy of the extracted fitting parameters. Additionally, all the fitting parameters are listed in Table S1, wherein the extracted CP energies (listed in Table 1 in paper) are given in bold for clarification. Note that, the error bar is determined by the difference between the average of the multiple fitting results and the best-match results we chosen for discussion.

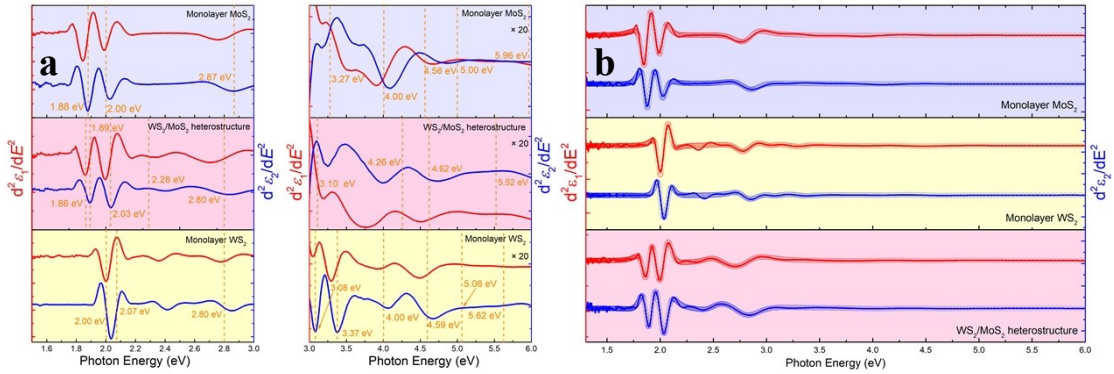

Fig. S7 CP determination. The red (blue) curves are the real (imaginal) part of second derivative of the complex dielectric functions ($d^2\varepsilon/dE^2$), respectively. The vertical dash lines in plot (a) locate the transition energies of CPs. The magnitude of photon energies ranging from 3.0-6.0 eV have been magnified by factor 20, because of their original small values. And the solid curves in plot (b) are obtained by numerical differentiation, while the unfilled symbols are the best matching curves (obtained via the SCP model).

Table S1 Fitting parameters of $d^2\varepsilon/dE^2$ for all the samples derived from SCP model (equation (5) in paper)

CPs	Parameters	A	B	C	D	E	F	G	H	I	J
MoS_2	A/no unit	0.83 ±0.134	0.83 ±0.068	4.53 ±0.019	2.91 ±1.869	2.39 ±0.626	4.15 ±0.664	3.80 ±1.201	4.781 ±0.219	\	\
	φ/deg.	160 ±131.0	125 ±67.3	156 ±22.0	139 ±115.9	147 ±113.7	151 ±83.5	165 ±7.0	184 ±51.0	\	\

WS_2	E_{th}/eV	**1.88 ±0.016**	**2.00 ±0.111**	**2.87 ±0.014**	**3.27 ±0.178**	**4.00 ±0.356**	**4.56 ±0.349**	**5.00 ±0.564**	**5.96 ±0.553**	\	\
	Γ/eV	0.08 ±0.006	0.08 ±0.006	0.47 ±0.225	0.67 ±0.412	1.02 ±0.614	1.23 ±0.453	1.17 ±0.742	0.38 ±0.306	\	\
	A/no unit	1.49 ±0.513	2.24 ±1.633	2.06 ±0.445	2.34 ±2.127	1.42 ±0.449	3.12 ±1.270	2.64 ±1.386	3.17 ±0.394	3.23 ±0.287	\
	φ/deg.	120 ±23.2	145 ±48.8	145 ±71.2	139 ±28.6	83 ±32.3	176 ±80.8	172 ±48.8	177 ±24.5	206 ±83.7	\
WS_2/MoS_2	E_{th}/eV	**2.02 ±0.015**	**2.40 ±0.024**	**2.82 ±0.207**	**3.09 ±0.015**	**3.20 ±0.097**	**3.70 ±0.330**	**4.36 ±0.075**	**4.50 ±0.458**	**5.75 ±0.764**	\
	Γ/eV	0.07 ±0.004	0.11 ±0.059	0.41 ±0.238	0.33 ±0.210	0.19 ±0.582	0.51 ±0.099	0.36 ±0.037	0.46 ±0.032	0.50 ±0.215	\
	A/no unit	1.84 ±0.327	1.21 ±0.080	1.54 ±0.319	4.32 ±0.717	3.54 ±0.765	1.24 ±0.612	2.73 ±1.134	2.94 ±1.303	2.77 ±0.405	2.42 ±0.003
	φ/deg.	171 ±109.10	240 ±49.36	286 ±25.16	183 ±166.32	172 ±50.22	170.69 ±141.76	192 ±14.0	219 ±3.3	107 ±36.27	62 ±1.34
	E_{th}/eV	**1.86 ±0.044**	**1.89 ±0.018**	**2.03 ±0.005**	**2.28 ±1.332**	**2.80 ±0.043**	**3.10 ±0.803**	**4.26 ±0.737**	**4.50 ±1.167**	**4.62 ±1.100**	**5.52 ±0.243**
	Γ/eV	0.11 ±0.023	0.10 ±0.003	0.10 ±0.006	0.34 ±0.170	0.36 ±0.048	0.83 ±0.002	0.27 ±0.011	0.51 ±0.201	0.27 ±0.025	0.03 ±0.014

5. Excitonic Properties Fitting

The discrete states of the exciton observed in 1L-TMDs and heterostructure thin films can be modelled using a broaden Lorentzian line shape. It is important to note that the maximum value of n during the fitting process is less than 8, due to the limitation of difficulty in calculation. Fig. S8 shows the best fitting curves and the measuring curves. As one can see that the fitting and measuring curves are consistent with each other in the whole range of photon energy. And the best fit results were summarized in Table S2, for legibility, the digitals of the transition energies (E_0) and the excitonic binding energies (E_b) are shown in bold. Note that, the error bar is determined by the difference between the average of the multiple fitting results and the best-match results we chosen for discussion.

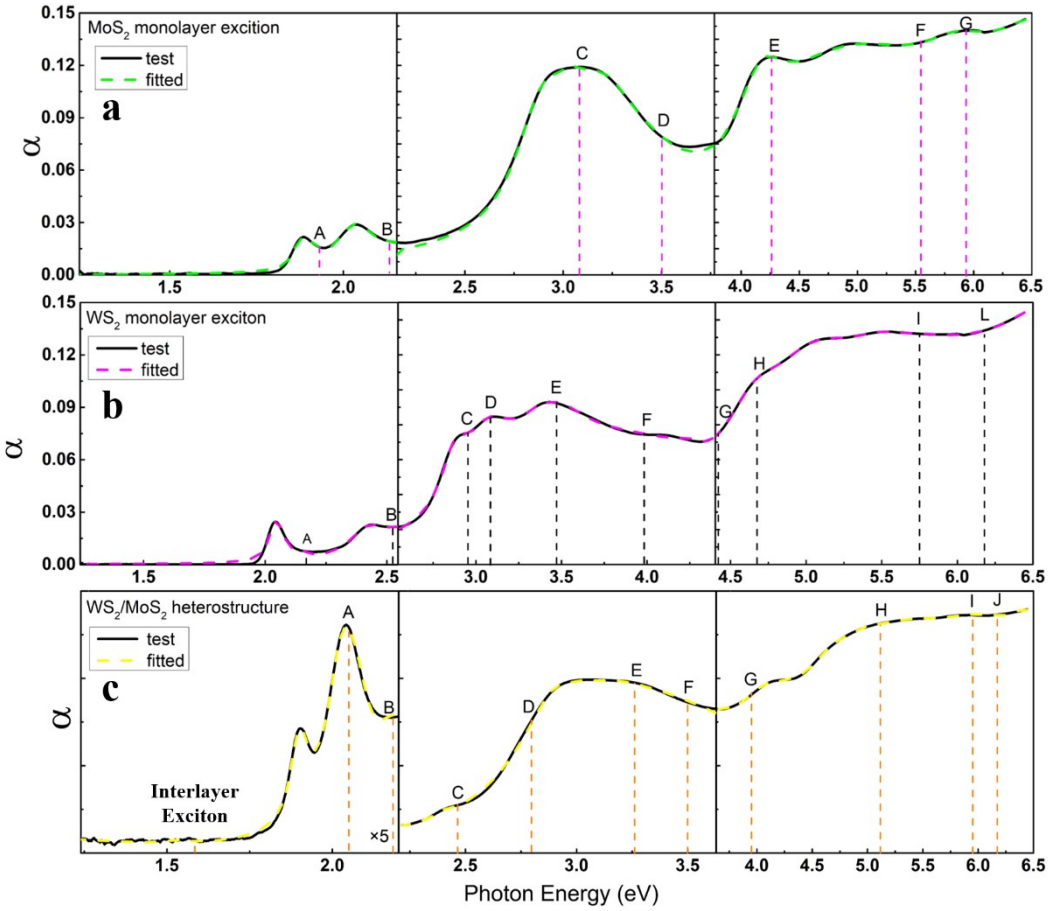

Fig. S8 Excitons obtained by fitting absorption coefficient spectrum ($\alpha(E)$) of (a) 1L-MoS_2, (b) 1L-WS_2 and (c) WS_2/ MoS_2 heterostructure. The solid (dash) curves represent the test (fitting) $\alpha(E)$ of the three samples. Vertical dash lines locate the transition energies of the excitons. For better legibility of the interlayer exciton, the heterostructure curves in the photon energy range from 1.24-2.20 eV is enhanced by a factor of 5.

Table S2 Fitting parameters of excitons of 1L-WS_2, 1L-WS_2, and WS_2/MoS_2 heterostructure thin films.

Excitons		Interlayer Exciton	A	B	C	D	E	F	G	H	I	J
MoS_2	A/eV nm^{-1}	\	2.68×10^{-3} ±0.002	1.94×10^{-3} ±0.0003	1.33×10^{-2} ±0.0004	2.45×10^{-2} ±0.003	2.09×10^{-2} ±0.0012	3.05×10^{-2} ±0.0035	6.39×10^{-2} ±0.0004	\	\	\
	E_0/eV	\	**1.93 ±0.004**	**2.16 ±0.008**	**3.49 ±0.141**	**3.69 ±0.095**	**4.25 ±0.053**	**5.55 ±0.393**	**5.92 ±0.385**	\	\	\
	E_b/meV	\	**676.35 ±11.625**	**475.80 ±223.084**	**748.08 ±8.110**	**296.63 ±60.867**	**506.37 ±126.342**	**475.07 ±223.805**	**122.41 ±197.044**	\	\	\
	Γ_1/meV	\	26.46 ±0.572	69.81 ±14.349	207.67 ±47.814	289.74 ±106.860	1151.56 ±137.475	239.30 ±934.454	805.28 ±395.797	\	\	\
	Γ_2/meV	\	21.60 ±7.979	35.48 ±2.075	143.84 ±8.812	128.50 ±121.391	25.55 ±388.431	974.12 ±973.820	1126.02 ±873.983	\	\	\
	Γ_3/meV	\	18.74 ±8.252	41.64 ±2.442	108.37 ±14.160	66.29 ±8.193	369.53 ±140.113	1273.843 ±1271.829	314.43 ±84.612	\	\	\
	Γ_4/meV	\	27.06 ±10.622	16.40 ±14.908	\	\	\	\	\	\	\	\
	Γ_5/meV	\	24.84 ±1.123	9.19 ±0.224	\	\	\	\	\	\	\	\
	Γ_6/meV	\	21.74 ±3.739	1.75 ±0.875	\	\	\	\	\	\	\	\
WS_2	A/eV nm^{-1}	\	8.14×10^{-4} ±0.0002	2.28×10^{-3} ±0.0001	7.29×10^{-2} ±0.079	4.05×10^{-2} ±0.003	1.18×10^{-1} ±0.002	2.18×10^{-2} ±0.003	5.20×10^{-2} ±0.022	1.85×10^{-1} ±0.174	1.94×10^{-2} ±0.019	8.32×10^{-2} ±0.026
	E_0/eV	\	**2.17 ±0.004**	**2.56 ±0.003**	**2.95 ±0.023**	**3.07 ±0.002**	**3.45 ±0.004**	**3.94 ±0.160**	**4.41 ±0.435**	**4.68 ±0.123**	**5.75 ±0.136**	**6.18 ±0.209**
	E_b/meV	\	**489.04 ±9.712**	**498.48 ±12.720**	**692.85 ±103.668**	**574.40 ±128.267**	**421.84 ±52.625**	**593.88 ±125.275**	**220.160 ±39.464**	**358.4 ±258.944**	**376.35 ±276.711**	**331.04 ±11.520**
	Γ_1/meV	\	33.58 ±0.035	106.21 ±0.390	512.70 ±0.303	159.91 ±79.956	941.96 ±883.92	317.00 ±66.576	839.41 ±419.706	673.17 ±26.819	917.97 ±82.031	1000.00 ±0.002
	Γ_2/meV	\	38.03 ±0.104	42.30 ±1.709	0.24 ±0.120	174.79 ±371.940	329.91 ±626.868	296.13 ±71.725	110.57 ±55.287	182.48 ±8.743	350.70 ±253.034	168.92 ±166.785
	Γ_3/meV	\	39.91 ±0.062	16.60 ±0.595	95.49 ±39.214	176.71 ±261.784	342.59 ±315.680	310.69 ±280.689	152.26 ±74.965	721.91 ±278.085	958.71 ±43.294	743.21 ±256.673
WS_2/MoS_2	A/eV nm^{-1}	4.38×10^{-4} ±0.0001	6.67×10^{-4} ±0.0005	1.83×10^{-3} ±0.0006	5.94×10^{-4} ±0.0002	6.87×10^{-3} ±0.0014	1.57×10^{-2} ±0.0002	2.84×10^{-2} ±0.0018	8.07×10^{-2} ±0.019	1.64×10^{-1} ±0.088	5.00×10^{-2} ±0.182	8.10×10^{-2} ±0.008
	E_0/eV	**1.58 ±0.050**	**2.05 ±0.054**	**2.20 ±0.026**	**2.47 ±0.001**	**2.80 ±0.089**	**3.27 ±0.060**	**3.50 ±0.087**	**3.94 ±0.045**	**5.10 ±0.302**	**5.95 ±2.329**	**6.18 ±0.506**
	E_b/meV	**431.39 ±127.818**	**604.88 ±129.116**	**597.52 ±45.856**	**306.77 ±40.044**	**374.48 ±227.978**	**343.07 ±112.247**	**364.97 ±121.657**	**301.23 ±232.634**	**328.24 ±25.850**	**204.33 ±42.865**	**51.36 ±25.634**
	Γ_1/meV	309.96 ±141.884	28.57 ±11.333	76.53 ±0.677	301.86 ±298.951	328.32 ±95.861	192.53 ±48.112	445.32 ±24.867	173.94 ±86.925	185.63 ±3.822	240.94 ±160.536	501.01 ±2.010
	Γ_2/meV	237.71 ±104.418	17.83 ±14.324	35.99 ±13.157	187.94 ±156.250	415.94 ±174.333	229.92 ±88.253	445.10 ±12.957	260.48 ±128.157	301.64 ±21.124	392.81 ±131.439	500.77 ±1.540
	Γ_3/meV	45.46 ±17.375	35.36 ±25.794	26.90 ±12.260	146.98 ±131.520	826.84 ±466.766	288.08 ±151.047	445.06 ±96.9	553.25 ±431.920	65.40 ±4.140	793.40 ±266.094	668.65 ±285.845

Reference

1 H. L. Liu, C. C. Shen, S. H. Su, C. L. Hsu, M. Y. Li, and L. J. Li, *Appl. Phys. Lett.*, 2014, **105**, 201905.

2 G. Wang, A. Chernikov, M. M. Glazov, T. F. Heinz, X. Marie, T. Amand and B. Urbaszek, *Rev. Mod. Phys.*, 2017, **90**, 021001.

3 P. Y. Yu, M. Cardona, *Fundamentals of Semiconductors: Physics and Materials Properties*, Springer, Heidelberg, 2010.

4 M. Grundmann, ed., *The Physics of Semiconductors*, Springer, Heidelberg, 2006.

5 C. Hamaguchi, ed., *Basic Semiconductor Physics*, Springer, Heidelberg, 2010.

6 J. E. Padilha, H. Peelaers, A. Janotti and C. G. V. Walle, *Phys. Rev. B*, 2014, **90**, 205420.

7 C. Cong, J. Shang, Y. Wang and T. Yu, *Adv. Opt. Mater.*, 2018, **6**, 1700767.

8 N. Peimyoo, W. Yang, J. Shang, X. Shen, Y. Wang, and T. Yu, *ACS Nano*, 2014, **8**, 11320–11329.

9 M. D. Tran, J. H. Kim and Y. H. Lee, *Cur. Appl. Phys.*, 2016, **16**, 1159-1174.

10 D. K. Zhang, D. W. Kidd and K. Varga, *Nano Lett*, 2015, **15**, 7002-7005.

11 A. Pant, Z. Mutlu, D. Wickramaratne, H. Cai, R. K. Lake, C. Ozkan and S. Tongay, *Nanoscale*, 2016, **8**, 3870-3887.

12 F. Ceballos, M. Z. Bellus, H. Y. Chiu, and H. Zhao, *Nanoscale*, 2015, **7**, 17523.

13 H. Chen, X. Wen, J. Zhang, T. Wu, Y. Gong, X. Zhang, J. Yuan, C. Yi, J. Lou, P. M. Ajayan, W. Zhuang, G. Zhang and J. Zheng, *Nat. Commun.*, 2016, **7**, 12512.

14 D. H. Li, H. Zheng, Z. Y. Wang, R. J. Zhang, H. Zhang, Y. X. Zheng, S. Y. Wang, D. W. Zhang and L. Y. Chen, *Phys. Chem. Chem. Phys.*, 2017, **19**, 12022-12031.

15 Y. Li, A. Chernikov, X. Zhang, A. Rigosi, H. M. Hill, A. M. Zande, D. A. Chenet, E. M. Shih, J. Hone, and T. F. Heinz, *Phys. Rev. B*, 2014, **90**, 205422.

16 T. Isaksson, and P. R. Griffiths, *Appl. Spectrosc.*, 2002, **56**, 916-919.